The Analysis of Various Size, Visually Selected and Density and Magnetically Separated Fractions of Luna–16 and –20 Samples

The Royal Society Luna Sample Investigation Team

G. Eglinton, A. P. Gowar, A. J. T. Jull, C. T. Pillinger
School of Chemistry, University of Bristol

S. O. Agrell, J. E. Agrell, J. V. P. Long
Department of Mineralogy and Petrology, University of Cambridge

S. H. U. Bowie, P. R. Simpson, R. D. Beckinsale, J. J. Durham
Institute of Geological Sciences, London

G. Turner, P. H. Cadogan
Department of Physics, University of Sheffield

T. C. Gibb, R. Greatrex, N. N. Greenwood
Department of Chemistry, University of Leeds

D. W. Collinson, S. K. Runcorn, A Stephenson
Department of Physics, University of Newcastle-upon-Tyne

S. A. Durrani, J. H. Fremlin, F. S. W. Hwang, H. A. Kahn[1]
Department of Physics, University of Birmingham

Samples of Luna 16 and 20 have been separated according to size, visual appearance, density, and magnetic susceptibility. Selected aliquots were examined in eight British laboratories. The studies included mineralogy and petrology, selenochronology, magnetic characteristics, Mössbauer spectroscopy, oxygen isotope ratio determinations, cosmic ray track and thermoluminescence investigations, and carbon chemistry measurements.

Luna 16 and 20 are typically mare and highland soils, comparing well with their Apollo counterparts, Apollo 11 and 16, respectively. Both soils are very mature (high free iron, carbide, and methane and cosmogenic ^{38}Ar), while Luna 16, but not Luna 20, is characterized by a high content of glassy materials. An aliquot of anorthosite fragments, handpicked from Luna 20, had a gas retention age of about 4.3 ± 0.1 Gy.

Two cores of lunar soil have been returned to Earth by the Soviet unmanned landers Luna 16 and 20. The Luna 16 core was collected in September 1970 from the northeastern part of the Mare Fecunditatis; Luna 20 landed in a typical highland region of the Moon at latitude 3°32′ W. and longitude 56°33′, near the crater Apollonius C. Both cores have been analyzed by Soviet workers (refs. 1 and 2) and by American and French consortia. (See *Earth Planetary Science Let-*

[1] On leave from Pakistan Institute of Nuclear Science and Technology (PINSTECH), Nilore, Rawalpindi, Pakistan.

ters, Vol. 13, pp. 225–466, and Vol. 17, pp. 3–63; and *Geochimica et Cosmochimica Acta*, Vol. 37, pp. 719–1110, and Vol. 37, pp. 1991–2035, for collected papers.)

Two 0.5g samples (L1627 and L2015, from the 27-cm level of zone B and from the 27- to 32-cm unit of the L16 and L20 cores, respectively) generously provided by the Soviet Academy of Sciences to the Royal Society, have been separated sequentially according to size, visual appearance, density, and magnetic susceptibility.

We report here the collaborative study of a number of selected aliquots by a consortium of eight British laboratories. A number of techniques not previously applied to Luna samples have been used. The investigations performed included mineralogy and petrology, selenochronology, magnetic properties, Mössbauer spectroscopy, thermoluminescence investigation, oxygen isotope ratio determinations, cosmic ray track and micrometeorite crater densities, and carbon chemistry measurements.

Experimental Studies

SAMPLE PROCESSING

All operations were performed in the clean room facility at the Organic Geochemistry Unit, University of Bristol (ref. 3). Sample manipulation was carried out with precleaned equipment. Glass spatulas (cleaned with aqua regia) or aluminium foil squares (toluene/methanol-extracted) were used for sample transfer. Storage vessels were either B14 Quickfit glass tubes (cleaned with aqua regia) or polystyrene vials (as supplied by Dr. M. B. Duke, Curator of Apollo Lunar Samples at the Lyndon B. Johnson Space Center, Houston). The sample processing

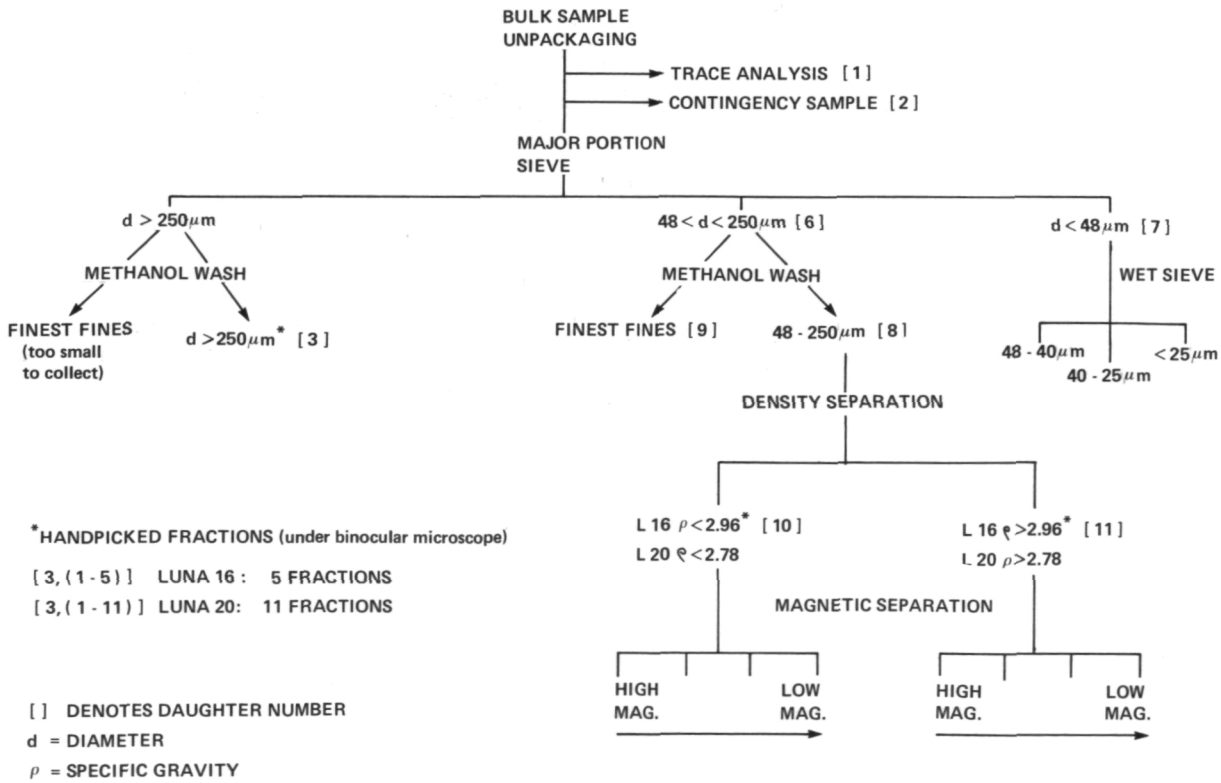

Figure 1.—*Separation scheme for processing Luna 16 and 20 fines.*

scheme adopted for both samples is outlined in figure 1; the sample distribution is shown in table 1. Material $> 250\mu$m was handpicked for further study under the binocular microscope according to the scheme outlined in tables 2 and 3.

ANALYTICAL PROCEDURES

The analytical procedures used in this study have been or will be described in detail elsewhere. Fractions of particles $> 250\mu$m and $< 48\mu$m were mounted and polished for microscopic and electron probe microanalysis in circular brass mounts of one-inch diameter, drilled to provide individual mounting positions in which each grain was firmly embedded in epoxy resin.

The mineral and rock compositions have been determined with an electron probe and energy-dispersive spectrometer. Spectrum deconvolution, peak integration, and matrix corrections were performed in a small on-line computer. In this procedure, uncertainties in estimation of background result in errors that vary in magnitude from element to element, and in limits of detection which are typically of the order of 0.05 percent except for sodium, where the rapidly increasing absorption of the 0.001″ Be window limits sensitivity to $\sim$ 0.3 percent. In most analyses, sodium values were below this limit.

Bulk rock compositions were measured by averaging the results of some 10 determinations carried out with an enlarged probe area. It must be emphasized that this procedure can introduce systematic errors of several percent (relative) in the case of the light elements in mixtures of plagioclase and a ferromagnesian mineral, and caution is necessary in any interpretation depending on differences in measured values of less than 5 percent.

Sample L2015,3,6 was irradiated with high fluence ($J = 0.1295$) of neutrons; the irradiation designated SH31 will be reported separately. Argon was extracted and analyzed (ref. 4) in 12 heating steps, of 30 minutes each step. Natural remanent magnetism (NRM) measurements were made with a small-scale magnetometer (ref. 5). Mössbauer spectra were recorded at room temperature (294 K) and at liquid nitrogen temperature (77 K), by use of the techniques developed for the Apollo 14 and 15 soils (refs. 6 and 7). Thermoluminescence data were recorded by heating 1-mg samples in an oxygen-free nitrogen atmosphere at 4°/s. The thermoluminescence emission spectrum induced by artificial radiations was analysed by the method of Durrani et al. (ref. 8) taking into account the efficiency of the (quartz window) photomultiplier and the transmission characteristics of the filter used. Oxygen isotopes were measured by conversion to carbon dioxide; the procedure is given in detail by Beckinsale et al. (ref. 9). Optical and scanning electron microscopes were used to study surface features, particularly impact craters and charged particle tracks. The deuterocarbon CD_4 (from deuterolysis of hydrolysable carbon phase) and the trapped hydrocarbon CH_4 were released from samples by deuterated acid dissolution (DCl, 38 percent in D_2O, Ciba Ltd.) and quantitated by gas chromatography (refs. 10 and 12).

Results and Discussion

PETROLOGY

Luna 16

The $> 250\mu$m grains previously selected under a binocular microscope were mounted, examined under a polarizing reflected light microscope, and reclassified.

Some of the soil breccia and agglutinate fragments broke up on mounting into separate fragments which were then individually classified. One of the "basaltic" fragments classified under the binocular proved, on further examination, to be an agglutinate. With this one exception, all fragments remained within their binocular class. Additional categories related to agglutinate were recognized (e.g., vesicular drops, glassy drops, and

Table 1.—*Sample Distribution* (1)

Sample Type	Daughter Number	Minerology and Petrology (Agrell and Bowie)	Seleno-chronology (Turner)	Magnetic (Runcorn)	Mössbauer Spectroscopy (Greenwood)	O Isotope (Beckinsale)	Thermo-Luminescence (Durrani)	Tracks (Durrani)	Carbon Chemistry (Eglinton)
Bulk Unseparated Material	1 or 2	–	–	–	+	–	–	–	+
d > 250μm Handpicked	3,1–5 (L16) 3,1–11 (L20)	+	L20*	+	–	–	–	+	L16*
d < 48μm	7	+	–	+	–	+	+	+	+
Unseparated 48 < d < 250μm	8	+	–	–	–	–	–	+	+
Finest Fines	9	+	–	+	L16*	–	–	+	+
48 < d < 250μm Light L16 < 2.96 L20 < 2.78	10	+	–	+	–	–	–	–	+
48 < d < 250μm; Heavy L16 > 2.96; L20 > 2.78	11	+	–	+	–	–	–	–	+
48 < d < 250μm; Light Magnetic Separates	10g,2	–	–	–	–	–	–	L16*	L16*
48 < d < 250μm; Heavy Magnetic Separates	11,2	–	–	–	–	–	–	L16*	L16*

NOTE: (1) Symbols used as follows: d = diameter of sample.
+ = samples of both L16 and L20 examined.
* = samples of only L16 or L20 examined.
– = no samples of either L16 or L20 examined.

Table 2.—*Luna 16: Classification Scheme of Handpicked Fragments > 250μm*

Section Number	Sample Number	Binocular Sample Classification	Column Number (with number of fragments of each type)							
			(1)	(2)	(3)	(4)	(5)	(6)	(7)	Total
1	L1627,3,B	Residual Fraction	3	11	1	5	3	1	1	25
2	L1627,3,2	Basaltic Fragments	1	0	0	1	0	0	0	2
3	L1627,3,3 (8)	Soil Breccia	1	2	0	0	1	0	0	4
4	L1627,3,5 (8)	Agglutinates	0	0	0	5	0	0	0	5
		Totals	5	13	1	11	4	1	1	36

NOTES: (1) Ilmenite Basalt
(2) Soil Breccia
(3) Glass-Coated Soil Breccia
(4) Agglutinate
(5) Vesicular Drop
(6) Glassy Drop
(7) Glassy Fragment
(8) These fragments broke up on mounting.

glassy fragments). Thirty-six fragments were studied, of which the greater part are soil breccias (13) and agglutinates (11). Ilmenite basalts are represented by five fragments. In the remaining categories there are four vesicular drops and one each of the following: glass-coated soil breccias, glassy drops, and glassy fragments.

The major particle types occurring in Luna 16 are discussed as follows:

Ilmenite Basalt: All five ilmenite basalt grains studied are characterized by a high proportion of ilmenite (about 10 percent) uniformly distributed throughout the basalt, which has well-developed ophitic texture. The largest handpicked fragment contains, in addition, notable phenocrysts of olivine intergrown with a pinkish spinel phase that does not occur elsewhere in the rock fragment. All other fragments studied appear olivine-free; but this may be a reflection of the small sizes of the fragments studied, since the olivine phenocrysts are widely separated in the ophitic groundmass. The order of crystallization for the basalts as a whole could therefore be summarized as phenocrysts of a spinel and olivine in a groundmass of feldspar, ilmenite, pyroxene, troilite, and iron, crystallizing in that order.

Soil Breccia: Thirteen soil breccia fragments were identified, two of them from the binocular soil breccia class, and the rest from the residual fraction. They comprise weakly aggregated soil clods that break up when touched. More detailed study reveals the presence of unsorted individual mineral grains of the ilmenite basalt suite and clasts comprising one or more basaltic minerals. In addition, angular or rounded grains of nickel-iron were observed. Glass is abundant in the breccia in a multiplicity of forms ranging from perfect spheres to angular fragments, intergranular permeations, and coatings on mineral grains, clasts, and rock fragments. One soil breccia fragment is notable for a glass coating on one side that links this category to that of the agglutinates.

Agglutinate: Nearly half the fragments studied are either agglutinates or a related fragment type such as vesicular drops,

Table 3.—*Luna 20: Classification Scheme of*

Section Number	Sample Number	Binocular Sample Classification	(1)	(2)	(3)	(4)
5	L2015,3,B	Residual Fractions	0	1	1	3
6	L2015,3,2	Fine Glassy Agglutinate	0	0	0	0
6	L2015,3,3	Glass-Coated Soil Breccia	0	0	0	0
7	L2015,3,4	Chalky Feldspar Shocked Friable	0	0	0	0
7	L2015,3,5	Vitreous Plagioclase	1	0	0	0
8	L2015,3,6	Microcrystalline Plagioclase Fragments	0	0	0	0
8	L2015,3,7	Coarsely Polycrystalline Plagioclase (15)	0	0	0	0
9	L2015,3,8	Microbreccias Pyroclastic Texture (15)	0	0	0	12
10	L2015,3,8	Microbreccias Pyroclastic Texture	0	0	0	0
		Totals	1	1	1	15

NOTES: (1) Partially Maskelynitized Anorthositic Granulite With Olivine
(2) Feldspathic Basalt
(3) Fine-Grained Feldspathic Soil Breccia
(4) Glass-Bonded Soil Breccia = Shock-Lithified Soil
(5) Splash Glass Invading Soil Breccia
(6) Agglutinate
(7) Very Fine Grained Pale Metaclastic Rock With Small Plagioclase Porphyroclasts

Handpicked Fragments > 250 μm

(see identifying notes) and Number of Fragments of Each Type										
(5)	(6)	(7)	(8)	(9)	(10)	(11)	(12)	(13)	(14)	Total
0	3	5	1	1	1	1	0	0	0	17
0	2	0	0	0	0	0	0	0	0	2
1	2	0	0	0	0	0	0	0	0	3
0	0	0	0	0	0	0	2	0	0	2
0	0	0	0	0	0	0	0	1	0	2
0	0	2	0	0	0	0	0	0	0	2
0	0	0	0	0	0	6	0	0	0	6
0	2	4	2	0	0	0	0	0	1	21
0	0	2	0	0	0	0	0	0	0	2
1	9	13	3	1	1	7	2	1	1	57

(8) Poikilitic Fragment of Noritic Affinity
(9) Anorthosite
(10) Devitrified Maskelynite
(11) High-Grade Noritic Metaclastic or Fine-Grained Impact Melt
(12) Shock-Melted Plagioclase
(13) Vitreous Pale Impact Melt
(14) Noritic Impact Melt With Subophitic Texture
(15) These fragments broke up on mounting.

glassy drops, or glassy fragments. The agglutinate is generally vesicular and in many cases has adherent microbreccia along one side of an agglutinate mass, and a smooth, rounded outline on the other. It contains partially digested mineral grains, notably ilmenite-basalt rock fragments and glassy fragments. A fine dissemination of iron and troilite spheres may be present in various sizes down to the resolution limit of the microscope. Vesicular drops, which are an agglutinate type with rounded or sub-rounded outline, lack adherent microbreccia but are otherwise similar to the agglutinate described above. In addition, a glassy drop and a glassy fragment are recorded. The glassy drop has a sub-rounded outline and contains less partially digested mineral fragments and clasts than the normal agglutinate. The polished surface of the drop in reflected light is distinctly mottled, which suggests inhomogeneity in the glass composition on the microscale. The glassy fragment has an angular but smooth outline with a few vesicles and mineral grains and clasts absent. The glass is optically homogeneous in reflected light, and is notable for the presence of many composite spheres of troilite and iron.

Luna 20

After preliminary sieving and handpicking, polished mounts were made from two fractions: 1 mg from the $< 48\mu$m fraction (L2015,7), and two fragments from each of the rock types recognized in the handpicked fraction $> 250\mu$m (L2015,3). Petrographic examination was undertaken, and the chemical composition of selected minerals and lithic and vitric fragments was determined.

Fraction $< 48\mu m$: A preliminary examination was made of a sample of the fraction $< 48\mu$m (L2015,7,2). Its composition was 65 percent angular mineral fragments (46 percent plagioclase, 18 percent ferromagnesian minerals, 1 percent oxide minerals) and 35 percent glassy fragments. The latter were equally divided between crystal-charged agglutinate and homogeneous glass free from inclusions. The mineral fragments were dominantly anorthite (An 95–98) with subordinate hypersthene.

Representative analyses are quoted in table 4. One fragment was recorded (analysis 3, table 4) of an aluminous hypersthene whose composition is suggestive of a high-pressure origin.

Representative glass analyses are quoted in table 5 and plotted on figures 2 and 3 along with the Luna 20 glass averages determined by Warner et al. (ref. 13). Of the glass analyses quoted, only three may be considered to have affinities with mare basalts or the melts which correspond to the end stage of their crystallization (analyses 3, 4, and 5, table 5). One silica glass was observed and all the rest are in the composition range of highland rocks. Too few analyses were made to delineate any population groupings within these glasses. But it should be noted that the majority have alumina and lime contents between the averages of the highland basalt and low-potassium Fra Mauro basalts of Warner et al. (ref. 13). It should also be noted that the composition of six of eight lithic fragments analyzed from the $> 250\mu$m fines of L2015 also fall in this composition range.

Fraction $> 250\mu m$: Polished mounts were made of two or three fragments of the several categories recognized in table 3, and from the residual material left over after the initial handpicking. These were reclassified after petrographic examination and electron probe analyses. The types recognized are summarized in table 3.

Mineral Fragments: The majority of the mineral fragments $> 250\mu$m were plagioclase; 10 were recognized in the original handpicking, and only one pyroxene was found.

The plagioclase may occur as clear colourless fragments with a vitreous lustre, as maskelynite, as devitrified maskelynite, and possibly as shock-melted material (analysis 5, table 4). Hypersthene (analysis 1, table 4) was represented by a single crystal showing cataclastic features.

The above are the only evidence in sample

L2015 for the existence of rocks with a grain size > 250μm at the Luna 20 site.

Lithic Fragments: All the fragments so far examined are of highland origin and no mare types have been recognized. The principal minerals recognized in these fragments are anorthite, hypersthene, olivine, augite with accessory ilmenite, iron metal, troilite, and spinel. In glassy fragments, or in fragments devitrified on the finest scale, metallic iron occurs as sporadic, rounded droplets usually < 2μm in diameter. In an agglutinate glass in L2015,3,3 one droplet was sufficiently large to analyze, and gave Ni 9.5 percent. In a glass-bonded soil breccia from L2015,3,B, nickel contents of from 5.8 percent to 11.2 percent were recorded in separate metal droplets. No two-phase metals were observed,

Table 4.—*Minerals from L2015*

	(1)	(2)	(3)	(4)	(5)	(6)	(7)	(8)	(9)	(10)
SiO_2	53.37	52.39	54.72	49.17	43.58	33.46	37.59	54.98	53.93	52.34
TiO_2	0.60	0.73	0.74	1.52	0.09	0.05	0.08	0.43	0.41	0.29
Al_2O_3	0.70	1.69	5.50	2.06	35.16	0.04	0.11	0.71	0.58	0.73
Cr_2O_3	0.56	0.61	0.76	0.19	0.00	n.d.	n.d.	n.d.	n.d.	n.d.
FeO	15.10	19.61	6.85	29.03	0.00	45.33	37.25	24.61	26.19	16.31
MnO	0.26	0.31	0.18	0.42	0.00	n.d.	n.d.	n.d.	n.d.	n.d.
MgO	25.47	22.31	32.47	10.55	0.00	20.89	25.89	17.24	17.99	15.10
CaO	1.92	2.47	0.48	8.15	19.71	0.10	0.46	1.96	3.71	14.42
Na_2O	n.d.[11]	n.d.	0.31	n.d.	0.30	n.d.	n.d.	n.d.	n.d.	n.d.
K_2O	n.d.	n.d.	n.d.	n.d.	0.04	n.d.	n.d.	n.d.	n.d.	n.d.
Total	97.98	100.12	102.01	101.09	98.88	99.93	101.41	99.93	102.81	99.19
Cations	0 = 6	0 = 6	0 = 6	0 = 6	0 = 8	0 = 4	0 = 4	0 = 6	0 = 6	0 = 6
Si	1.972	1.939	1.866	1.921	2.040	0.983	1.033	2.0009	1.996	1.988
Ti	0.017	0.020	0.019	0.045	0.003	0.001	0.002	0.012	0.012	0.008
Al	0.030	0.074	0.221	0.094	1.940	0.001	0.004	0.031	0.025	0.032
Cr	0.016	0.018	0.020	0.006	—	—	—	—	—	—
Fe	0.466	0.607	0.195	0.948	—	1.113	0.856	0.898	0.809	0.518
Mn	0.008	0.009	0.005	0.014	—	—	—	—	—	—
Mg	1.402	1.230	1.650	0.614	—	0.915	1.060	0.938	0.992	0.855
Ca	0.076	0.098	0.017	0.341	0.989	0.002	0.009	0.077	0.147	0.587
Na	—	—	—	—	0.027	—	—	—	—	—
K	—	—	—	—	0.002	—	—	—	—	—
Fe	24.0	31.3	10.5	49.8	Ca97.1	Fe 54.9	44.7	47.0	41.5	26.4
Mg	72.1	63.6	88.6	32.3	Na 2.7	Mg45.1	55.3	49.0	50.9	43.6
Ca	3.9	5.1	0.9	17.9	K 0.2	Ca —	—	4.0	7.6	30.0

NOTES: (1) Hypersthene crushed fragment from L2015,3,10 associated with minor anorthite.
(2) Hypersthene fragments from < 48μm fraction L2015,7,2.
(3) Aluminous hypersthene < 48μm fraction L2015,7,2.
(4) Ferroaugite < 48μm fraction L2015,7,2.
(5) Plagioclase, annealed shock-melted plagioclase with small irregular gas cavities from L2015,3,4,1.
(6) Olivine includes NiO 0.06 percent.
(7) Olivine includes NiO 0.03 percent.
(8) Hypersthene
(9) Hypersthene
(10) Augite
(11) n.d. = Not detected.

(6)–(10): Melt rock with equigranular texture. Plagioclase ~ 70 percent; Ferromagnesians ~ 30 percent. L2015,3 B,11 Geoscan Analysis P.R.S.

Table 5.—*Analyses of Glassy or Microcrystalline Fragments < 48μm in Diameter, L2015,7,3*

	(1)	(2)	(3)	(4)	(5)	(6)	(7)	(8)	(9)
SiO_2	43.20	45.70	42.58	48.79	58.91	44.23	44.17	97.82	46.12
TiO_2	0.21	0.31	5.34	0.32	0.40	0.07	0.40	0.26	0.77
Al_2O_3	24.44	25.54	13.83	22.90	22.07	32.07	25.33	1.19	21.18
Cr_2O_3	0.21	0.09	0.21	0.00	0.07	0.07	0.23	0.00	0.21
FeO	5.94	5.69	17.55	11.05	7.11	1.79	6.09	0.07	9.40
MnO	0.08	0.05	0.21	0.16	0.09	0.00	0.00	0.00	0.09
MgO	8.73	8.74	8.23	0.00	0.66	3.73	6.76	0.00	6.64
CaO	14.31	14.62	10.62	13.49	11.55	17.62	14.52	0.00	15.31
Na_2O	0.30	n.d.	n.d.	0.44	n.d.	n.d.	0.59	n.d.	n.d.
K_2O	0.03	0.03	0.07	0.28	0.70	0.03	0.20	0.03	0.03
Total	97.45	100.74	98.64	97.43	101.56	99.76	98.29	99.37	99.72
CIPW NORM									
QZ	—	—	—	8.68	24.8	—	—	97.70	0.05
COR	—	—	—	—	0.31	—	—	1.16	—
OR	0.18	—	0.41	1.65	4.12	—	1.18	0.18	—
AB	2.54	—	—	3.72	—	—	4.99	0.01	—
AN	65.25	69.68	37.53	59.68	57.30	87.50	65.88	—	57.78
Dl	4.64	2.30	12.60	6.46	—	0.65	5.02	—	15.02
HY	8.67	21.28	37.08	16.63	14.14	9.52	7.85	—	25.08
OL	15.46	6.75	0.57	—	—	1.85	12.28	—	—
CM	0.31	0.13	0.31	—	0.10	0.10	0.34	—	0.31
IL	0.40	0.59	10.14	0.61	0.76	0.13	0.76	0.15	1.46
FS/HY Mol%	26.9	25.8	46.7	100.0	85.0	20.31	31.8	—	42.37

NOTES: (1) Colourless glassy fragments
(2) Colourless glassy fragments
(3) Pale brown glassy fragments
(4) Pale brown glassy fragments
(5) Pale brown agglutinate
(6) Colourless microcrystalline fragments
(7) Colourless microcrystalline fragments
(8) Fragment of silica glass
(9) Very pale brown glassy agglutinate

but a skin of troilite was observed in one case.

The majority of the lithic fragments are very fine grained (< 15μm) and are probably derived by shock lithification of the finest fractions of an incoherent lunar soil, the clastic origin of the recrystallized or vitrified material being inferred from the presence of small, angular porphyroclasts of plagioclase or—more rarely—olivine, up to 75μm in size.

Glass-bonded soil fragments, crowded with minute fragments of plagioclase and subordinate ferromagnesian minerals, occur as the least modified material. They grade into agglutinates with increase in the amount of glass and the development of an exterior glassy skin. These fragments are often incoherent and composite. One such fragment (table 3, section 9) broke up to reveal an inclusion of pale, recrystallized, feldspathic metaclastic rock with allotriomorphic granular texture and another with fine poikilitic texture and noritic composition.

The majority of the fine-grained, holocrystalline fragments have one of two principal

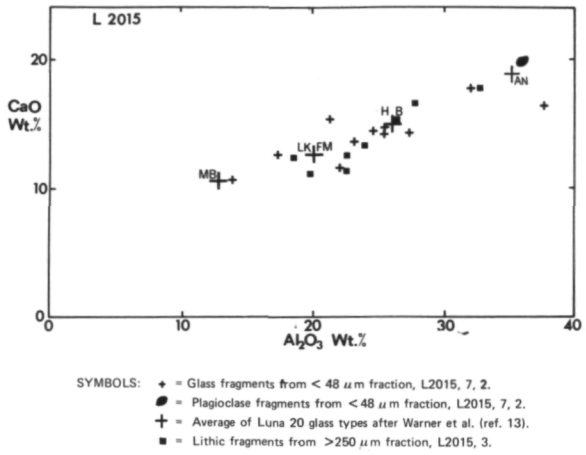

Figure 2.—*Plot of weight percent CaO versus weight percent Al_2O_3 for glass and lithic fragments from Luna 2015.*

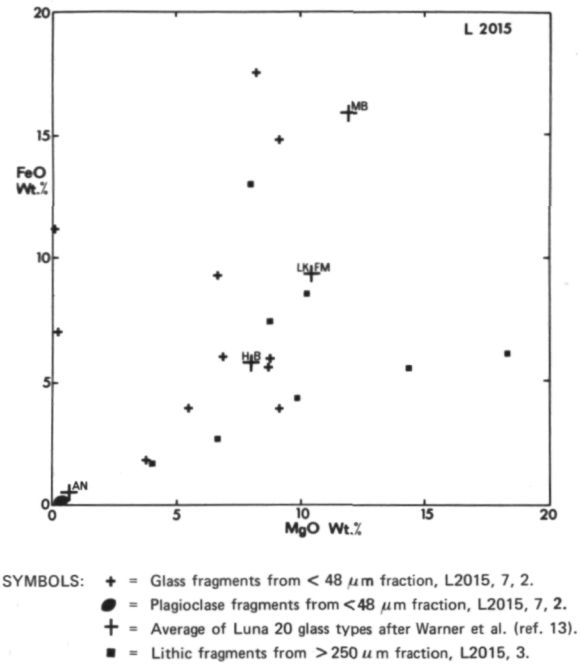

Figure 3.—*Plot of weight percent FeO versus weight percent MgO for glass and lithic fragments from Luna 2015.*

textures, either hypidioblastic granular or poikiloblastic. In the former, when hypersthene is about equal to plagioclase in amount, the hypersthene occurs as rods set in allotriomorphic plates of plagioclase. In more feldspathic fragments the plagioclase forms plate-like crystals and the pyroxene, allotriomorphic interstitial crystals.

Poikiloblastic textures characterize some of the more recrystallized fragments in which plagioclase does not greatly exceed hypersthene in amount. Hypersthene occurs in oikocrysts up to 30μm in size, including 5μm crystals of plagioclase. It is possible that these are direct crystallization products of an impact melt rather than the products of annealing of impact-produced glass.

Fragments with a granulitic texture are rare; one such fragment was studied (analysis 8, table 6). It is anorthositic in composition and made up of partially maskelynitized polygonal crystals of plagioclase with sporadic interstitial crystals of olivine (Fo81).

Another fragment (L2015,3,B,11) may be igneous or metamorphic: it has equigranular texture with $\sim$ 80 percent plagioclase, $\sim$ 10 percent pyroxene, and $\sim$ 5 percent olivine. The analyses of the pyroxenes and olivines are quoted in table 4, analyses 6–10. The fragment shows a unique texture in which sub-rounded crystals of olivine include blebs of 2μm of metallic iron just within their margins. Their small size precludes quantitative analysis, but they are probably nearly pure iron blebs with less than 0.2 percent nickel. The restriction of the metal drops within the margin of the olivine suggests that they are not just inclusions but are the products of some reducing reaction similar to that observed in the basalt 14053 described by El Goresy et al. (ref. 14). Here the olivine is not nearly pure fayalite but Fo45, Fa55, so that reaction products other than Fe and SiO_2 should be observed. Further work is being undertaken on this fragment.

The chemical composition of the lithic fragments was obtained by defocused beam analysis with the electron probe, and the results are set out in table 6 along with their CIPW NORMS. Reference to figures 2 and 3 and to table 5 shows the general chemical similarity of the lithic clasts to the glass fragments in the < 48μm fraction. Only one

Table 6.—*Microprobe Analyses of Fne-Grained Lithic Fragments From L2015*

	(1)	(2)	(3)	(4)	(5)	(6)	(7)	(8)
SiO_2	45.9	46.6	44.5	46.0	43.6	45.3	44.9	44.1
TiO_2	0.6	0.2	0.2	0.8	0.1	0.1	0.1	n.d.
Al_2O_3	23.8	22.2	22.3	18.4	19.8	28.2	26.1	32.3
Cr_2O_3	0.2	0.2	0.2	0.5	0.4	0.2	0.2	0.1
FeO	7.4	8.5	5.5	13.2	6.1	2.7	4.3	1.7
MnO	0.1	0.1	0.1	0.2	0.1	n.d.(9)	0.1	n.d.
MgO	8.7	10.5	14.5	8.2	18.6	6.6	9.7	3.9
CaO	13.2	11.3	12.8	12.7	11.3	16.8	14.7	17.9
Na_2O	n.d.	0.4	n.d.	n.d.	n.d.	n.d.	n.d.	n.d.
K_2O	0.1	n.d.	n.d.	n.d.	n.d.	n.d.	n.d.	n.d.
Total	100.0	100.0	100.0	100.0	100.0	100.0	100.0	100.0
CIPW NORM								
QZ	—	—	—	—	—	—	—	—
COR	—	0.2	—	—	—	—	—	—
OR	0.1	—	—	—	—	—	—	—
AB	—	3.4	—	—	—	—	—	—
AN	64.9	55.6	60.8	49.9	54.8	77.0	71.2	88.2
Dl	0.1	—	1.6	10.6	0.6	4.6	1.3	0.3
HY	30.8	30.1	15.8	34.5	11.8	14.8	16.2	7.6
OL	2.5	7.8	20.7	2.2	32.0	2.9	10.7	3.6
CM	0.3	0.3	0.3	0.7	0.5	0.2	0.3	0.2
IL	1.2	0.4	0.4	1.5	0.3	0.3	0.2	—
FS/HY.	30	30	27	46	15	17	19	20
Mo 1 percent								

NOTES: (1) L2015,3,10,B1: Fine-grained noritic metaclastic with minipoikilitic texture; $Na_2O < 0.3$ percent.
(2) L2015,3,11,D: Mean of 1–15 areas. Fine-grained noritic metaclastic with minipoikilitic texture.
(3) L2015,3,10,B: Shock-melted soil with 25μm plagioclase porphyroclasts; $Na_2O < 0.30$, $K_2O < .04$ percent.
(4) L2015,3,10,A: Shock-melted soil or agglutinate, cryptocrystalline; $Na_2O < 0.30$ percent, $K_2O < .04$ percent.
(5) L2015,3,5,2: Pale vitreous impact melt with residual olivine; $Na_2O < 0.3$ percent, $K_2O < 0.03$ percent.
(6) L2015,3,6,1: Fine-grained pale metaclastic; $Na_2O < 0.3$ percent, $K_2O < 0.03$ percent.
(7) L2015,3,7,1: Fine-grained impact melt; $Na_2O < 0.3$ percent, $K_2O < 0.03$ percent.
(8) L2015,3,5,1: Partially maskelynitized anorthositic granulite; $Na_2O < 0.3$ percent, $K_2O < 0.03$ percent.
(9) n.d. = In each use, indicates below limit of detection, all analyses normalized to 100 percent.

of the lithic fragments, a shock-melted soil or agglutinate (analysis 4, table 5) can be considered as possibly containing a mare-derived component. Its higher FeO (13 percent) and significant normative diopside (10.6 percent) distinguish it from all the other fragments which are of unambiguous highland origin. The latter fragments have the range of compositions found in clastic rocks and glasses of highland regions. Their normative mineralogy is variable, with anorthite from 55 to 90 percent, hypersthene from 7 to 30 percent, olivine from 3 to 30 percent, and diopside from 0 to 5 percent,

and less than 1 percent opaque minerals. The ferromagnesian minerals have a Fe/Fe+Mg ratio < 0.3.

Insofar as it is possible to determine the modal mineralogy of these fine-grained fragments, there is general agreement with the results obtained from the norm. It is apparent that these fragments were once the finer grained portions of highland soils and that they must have primary igneous parents, even if they are several generations removed. Igneous rocks of the ANT suite of anorthosites, norites, troctolites, and their intermediate variants are ultimately parental to the fine-grained fragments composing the $> 250\mu$m fraction of L2015.

SELENOCHRONOLOGY

The analysis of a single 8.7-mg fragment of glassy and friable feldspar (L2015,3,1) has been reported previously (ref. 4). The sample was an extremely unfavorable one for dating, containing only 50 ppm K. An imprecise age of (4.0 ± 0.3) Gy was determined, the uncertainties arising from the small amount of sample gas and the large Ca and trapped ^{40}Ar corrections. This age is comparable to ages from other highland sites and to the ages of two K-rich metaclastic rocks from the Luna 20 site (ref. 15) but is too inaccurate to draw any significant conclusions. The nominal (^{38}Ar-^{37}Ar) exposure age of L2015,3,1 was accurately determined as 340 m.y. and is typical of the exposure age of fragments from a mature regolith.

More recently, a ^{40}Ar-^{39}Ar analysis of five fragments of microcrystalline plagioclase L2015,3,6 (total weight 7.7 mg) has been carried out. The potassium content of L2015,3,6 was 180 ppm, a factor of 3 higher than L2015,3,1, and this, coupled with improvements in the analytical technique, permitted the argon composition to be determined with greater precision.

Although the interpretations of the L2015, 3,6 results are not limited by analytical precision, there remains the problem of trapped ^{40}Ar. This is apparent in figure 4 where the results are plotted on a three-isotope correlation diagram of (^{36}Ar$_t$/^{40}Ar) against (^{39}Ar/^{40}Ar). A correction for cosmogenic ^{36}Ar has been applied on the basis of the (^{36}Ar/^{38}Ar) ratio, assuming a binary mixture of cosmogenic argon, $(^{36}\mathrm{Ar}/^{38}\mathrm{Ar})_c = 0.63$, and trapped argon, $(^{36}\mathrm{Ar}/^{38}\mathrm{Ar})_t = 5.35$. It was assumed that cosmogenic ^{40}Ar would be negligible in samples of anorthositic composition due to the low Fe and Ti content. The effect of the correction is shown by the solid circles, which are the uncorrected ratios. On this diagram pure, trapped argon would plot on the axis (^{39}Ar*/^{40}Ar) $= 0$; pure, potassium-derived argon would plot on the axis (^{36}Ar/^{40}Ar) $= 0$. The experimental points represent a mixture of these components. The fact that the points

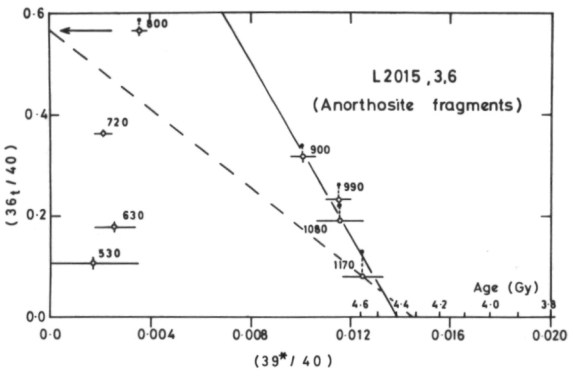

Figure 4.—*Three-isotope correlation plot (^{36}Ar$_t$/^{40}Ar) against (^{39}Ar*/^{40}Ar), for lunar sample L2015,3,6. The extraction temperatures are indicated in °C. The solid black circles indicate the (^{36}Ar/^{40}Ar) ratio before applying the correction for cosmogenic ^{36}Ar. Because the samples are anorthositic, cosmogenic ^{40}Ar is assumed to be negligible. The low-temperature points indicate unambiguously that the (^{36}Ar/^{40}Ar)$_t$ ratio of trapped gas increases with increasing extraction temperature to 800°C. The four high-temperature extractions represent 80 percent of the radiogenic argon release and, on the assumption that they are a binary mixture of trapped and radiogenic argon of fixed composition, indicate a K-Ar age of (4.4 ± 0.1) Gy (solid mixing line). The somewhat weaker assumption that the trapped (^{40}Ar/^{36}Ar)$_t$ ratio for the high-temperature points is greater than or equal to that 800° C extraction implies that the apparent age for the final extraction is not less than (4.3 ± 0.1) Gy (dashed line shows limiting case).*

are not colinear implies that there is no unique composition for either or both of the end members. Nevertheless, a number of important statements about the chronology of L2015,3,6 may be made, and two interpretations of figure 4 are possible.

The four high-temperature points represent 80 percent of the argon release from the sample and, within the analytical errors, are colinear. If this is a simple binary mixing line it corresponds to a trapped argon composition with $(^{40}Ar/^{36}Ar_t) = 0.8 \pm 0.2$ and the intercept with the $(^{39}Ar^*/^{40}Ar)$ axis corresponds to a K-Ar age of (4.4 ± 0.1) Gy. If the interpretation is correct, this would represent one of the oldest K-Ar ages determined on a lunar sample, and significantly older than other dated Luna 20 samples (ref. 15). Whether the high-temperature argon is a binary mixture or not, the composition of the low-temperature argon can *only* be understood in terms of excessive amounts of trapped ^{40}Ar in the initial argon release. The $(^{40}AR/^{36}Ar)_t$ ratio of this trapped component decreases *monotonically* from a value of around 10 in the 530° C fraction to < 1.8 in the 800° C fraction.

An alternative interpretation of figure 4 would regard the colinearity of the high-temperature points as fortuitous. In this case, it is necessary to make other assumptions about the trapped argon composition of the high-temperature points. A reasonable assumption would seem to be that the $(^{40}Ar/^{36}Ar)_t$ ratio decreases monotonically with temperature throughout the experiment, and that for the high-temperature points it is *less than or equal to* that of the 800° C release. This implies $(^{40}Ar/^{36}Ar)_t \leq 1.8$ or $(^{36}Ar/^{40}Ar)_t \geq 0.56$ for all temperatures above and including 800° C. The assumption provides a lower limit to the apparent age associated with each heating step. (This value is close to the 2.15 ± 0.22 ratio obtained by Podosek et al. (ref. 15) for a Luna 20 soil fragment.) The reader can see for himself, using figure 4 and a ruler, laid to pass through $(^{36}Ar/^{40}Ar)_t = 0.56$ and each experimental point in turn, that this assumption corresponds to a monotonically increasing apparent age for the high-temperature points. It is also clear that while the 900° C–1080° C points can yield apparent ages less than or equal to 4.1 Gy, the apparent age of the 1170° C point must be greater than (4.3 ± 0.1) Gy. The apparent age of the 1170°C point can only be as low as 4.0 Gy if the $(^{40}Ar/^{36}Ar)_t$ ratio *rises*, by a factor of 2, to (3.7 ± 0.5) in the final extraction. It is therefore difficult to avoid the conclusion that the argon released in the 1170° C fraction is coming from a very old sample.

In spite of uncertainties in the composition of the trapped argon, L2015,3,6 appears to contain a component which has retained argon from the period prior to 4.3 Gy and possibly since 4.4 Gy. The conclusions, it should be stressed, are based on measurements on a sample which is a mixture of anorthosite fragments with presumably different histories. Nevertheless, the presence of an old component in the Luna 20 soil is suggested. The application of the $^{40}Ar/^{39}Ar$ technique to sufficiently large, single fragments of anorthosite may identify this component.

The cosmogenic $(^{38}Ar/^{37}Ar)$ ratio in L2015,3,6 shows variations which reflect different exposure histories for the fragments. The variations correspond to exposure ages in the range from 400 to 700 m.y., which are typical of fragments from a mature regolith.

MAGNETIC MEASUREMENTS

The natural remanent magnetism (NRM) of two rock fragments has been investigated. L2015,3,1 (11.3 mg) was a whitish, angular chip of glassy feldspar with some black, crystalline inclusions. The NRM of the fragment was $< 3.5 \times 10^{-7}$ G. cm^3. g^{-1} and there was no detectable growth of viscous remanent magnetism in a weak field. The black inclusions are magnetic to the extent that they show susceptibility effects, with susceptibility in the range from 10^{-2} to 10^{-3} G. cm^3. g^{-1}. Oe^{-1}. However, this value, together with the fact that no detectable iso-

thermal remanence was acquired in a high field (3500 Oe), suggests that there is a negligible amount of iron in L2015,3,1 and that the black material does not contribute to the NRM.

L2015,3,11 (6.6 mg) was a breccia fragment with sparsely distributed black, opaque material visible in the surface. The magnetic remanence of this fragment is less than the minimum remanence detectable with the magnetometer used (about 40×10^{-6} G. cm^3. g^{-1}) (ref. 5). The shape of the isothermal remanence versus field curve was very similar to that obtained from similar Apollo samples, as was the saturation intensity, 0.97×10^{-3} G. cm^3. g^{-1}. Thus, magnetically, L2015,3,11 appears to be very much like breccias returned by the Apollo missions.

Several samples of fines were investigated (table 7), including density separates L1627, 10,1; L1627,11,1; L2015,10,1; and L2015, 11,1. Measurement of the room-temperature, low-field susceptibility yielded results which were similar to values found for Apollo fines (ref. 16). However, the susceptibilities of the Luna 16 samples were about a factor of 4 stronger than those of the Luna 20 samples. The density separation is remarkably effective in separating out a strong magnetic component which is present in the lighter fraction; for both Luna 16 and 20 samples, the light fraction was about 2.6 times as strong in susceptibility as the heavy fraction. A Curie point determination on L2015,10,1, sealed in an evacuated quartz tube and using a field of 8 kOe, indicated the presence of metallic iron ($T_c \sim 770°$ C), as in the case of Apollo fines samples. Also similar to the Apollo fines samples, the induced moment decreased to 54 percent of its initial value after heating, presumably due to partial oxidation (ref. 17).

The acquisition of isothermal remanent magnetization (IRM) was measured for density separates. At 4000 oersteds, the samples were within 7 percent of saturation (IRM_S), the extrapolated saturation values being shown in table 7. The Luna 16 samples were stronger in IRM than the Luna 20 samples by a factor of about 4.5; the light fractions were about 2.1 times as strong in IRM as the heavy fractions. Five further fines

Table 7.—*Room Temperature Values of Initial Susceptibility (X_i), Extrapolated Saturation IRM (IRM_s) and Induced Magnetization in 10 kOe (J_i)*

Sample	Description	X_i (10^{-3}G•cm^3•g^{-1}•Oe^{-1})	IRM_s (10^{-3}G•cm^3•g^{-1})	J_i (10 kOe) (G•cm^3•g^{-1})
L1627,10,1	Light (1) Fraction, 48 < d < 250μm	3.9	156	1.98
L2015,10,1	Light (1) Fraction, 48 < d < 250μm	1.0	36	0.42
L1627,11,1	Heavy (2) Fraction, 48 < d < 250μm	1.4	77	1.44
L2015,11,1	Heavy (2) Fraction, 48 < d < 250μm	0.4	17	1.24
L1627,3	Handpicked Fraction, d (3) > 250μm)	1.7	88	1.12
L1627,7	d < 48μm	2.7	97	1.02
L2015,7	d < 48μm	0.9	31	0.57
L1627,9	Finest Fines (d < 10μm)	4.0	149	1.89
L2015,9	Finest Fines (d < 10μm)	0.9	31	1.26

NOTES: (1) Light Fractions: L1627, < 2.96 g/cm^3; L2015, < 2.78 g/cm^3
(2) Heavy Fractions: L1627, > 2.96 g/cm^3; L2015, > 2.78 g/cm^3
(3) Diameter

samples (see table 7) were also measured. These had IRM curves identical in shape to the density-separated samples and to the Apollo 11 fines (ref. 16), suggesting that the various fractions contained essentially the same iron particle sizes. For seven of the nine samples, the induced magnetization failed to reach saturation in fields of 12 kOe. This behavior indicates the presence of paramagnetism or very small superparamagnetic particles. Samples L2015,7 and L2015,10,1, however, were saturated in fields of about 4 kOe, indicating the absence of this component. Larger superparamagnetic particles are, however, undoubtedly present in L2015,10,1 and the other density-separated samples (other samples were not measured) since their saturated IRM decayed logarithmically at approximately 4.5 percent per decade. Logarithmic decay is caused by relaxation of that part of the magnetic spectrum of the single domain grain distribution on the superparamagneticstable boundary (i.e., diameter about 130 Å). Apollo 11 fines (susceptibility $X_c = 2.4 \times 10^{-3}$ G. $cm^3.g^{-1}.Oe^{-1}$) contained 0.9 percent ($\pm$ 0.3 percent) of single domain iron grains (ref. 17). Assuming that the single domain iron content, most of which is in the superparamagnetic state with grain size less than about 130Å is proportional to the susceptibility, then the iron content of various Luna fractions may be estimated (using the Apollo 11 figures) from the susceptibility results in table 7.

MÖSSBAUER SPECTROSCOPY

The iron-bearing minerals in two unseparated 40-mg samples from the original bulk fines (L1627,2 and L2015,2) have been characterized by ^{57}Fe Mössbauer spectroscopy. A 2-mg separate of the very small particles from Luna 16 (finest fines, L1627,9) has also been studied.

The spectra (fig. 5) are very similar to those described by Malysheva (ref. 18) for Luna 16 sample 3–1; however, experience with Apollo 14 and Apollo 15 samples suggests somewhat different assignment of the central components of the spectra. It has become common practice to attribute the three apparent quadrupole doublets, in order of decreasing quadrupole splitting, to M1 pyroxene/olivine, M2 pyroxene/glass, and ilmenite.

From a close study of the data from both lunar and terrestrial pyroxenes and olivines it has been found that the M1 pyroxene/olivine content is best estimated from the area of the outer pair of peaks at 77 K, and the ilmenite content from the area of the inner pair of peaks at 295 K; the residual area is then attributed to M2 pyroxene/glass.

The greater intensity of the M2 pyroxene/glass component at lower velocity found in previous lunar samples has also been observed in the present study. The asymmetry has

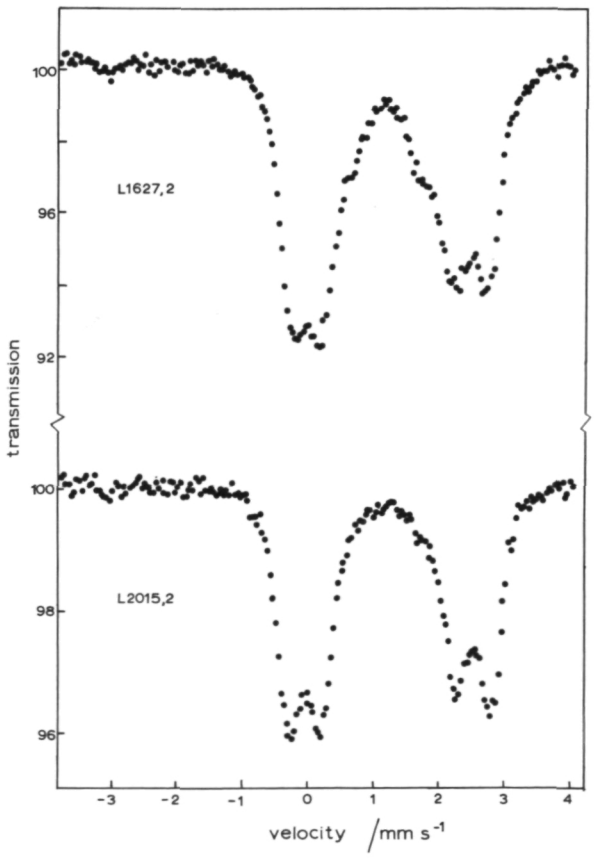

Figure 5.—*Mössbauer spectra of Luna 16 and 20 soils recorded at 77 K.*

Table 8.—*Distribution of Iron Among Various Phases Expressed as a Percentage of Total Iron*

Sample	M1/Olivine	M2/Glass	Ilmenite	Magnetic Iron	Other Iron
Luna 1627,2	32	53	6.9	~5	3.9
Luna 2015,2	41	52	<0.2	<2	4.2
Apollo 14 (average of 4)	17	64	8	~4	6
Apollo 15 (mare and front)	26	63	2.4	4.1	4
Apollo 15 (rille edge)	36	57	1.3	<2	3

already been shown to be greatest in samples with a significant enrichment in magnetic iron (ref. 7); thus, the greater part of it must originate from superparamagnetic inclusions of iron or iron-nickel alloy. To test this idea further, the separated sample L1627, 9 has been studied. The spectrum shows lines which are both less well resolved and more asymmetric than those in the spectra of the bulk samples. It is therefore consistent with the presence of a greater proportion of glassy particles and superparamagnetic iron in the separate.

Because of the uncertainty introduced by this component, the analysis shown in table 8, which compares the present results with earlier data on other lunar samples, is based on the area of the high-velocity peaks only. The results for magnetic iron are approximate because of the difficulty of estimating areas of weak lines broadened asymmetrically by the nickel content.

Both Luna samples exhibit relatively high M1 pyroxene/olivine contents in comparison with the Apollo 14 soils, and detailed analysis suggests that this indicates more augite and less pigeonite and orthopyroxene (rather than an excess of olivine). The samples resemble the Apollo 15 rille-edge materials except for the high ilmenite content of Luna 16. The ilmenite content of L2015,2 is so small as to be almost undetectable in the inner wings of the pyroxene absorption, and this is compatible with the TiO_2 analysis (0.56 percent in Luna 20 as against 3.39 percent in Luna 16 (ref. 13), some of which will be present in non-iron-containing phases). The Luna 16 sample shows a much greater magnetic iron/iron nickel component than the Luna 20 sample, but neither sample gives a significant resonance from species containing troilite or iron (III). The Mössbauer lines for the Luna 20 sample are significantly narrower than those for Luna 16, suggesting a lower glass content or smaller compositional variation in the Luna 20 sample. During the course of this work, other Mössbauer studies on Luna 16 (ref. 19) and Luna 20 samples (refs. 20 and 21) have been reported, and in general the results are in good agreement with the present data. However, the assignment (refs. 20 and 21) of weak peaks in the Luna 20 spectra to ulvospinel (Fe_2TiO_4) is questionable. The resonance lines from iron-titanium spinels are likely to be indistinguishable from those of iron atoms in the M2 pyroxene sites at room temperature (ref. 22). Since ulvospinel is magnetic at low temperature, significant changes should be present in the 77 K spectrum; such changes have not been observed.

THERMOLUMINESCENCE

Two Luna samples < 48 μm in diameter (L1627,7 and L2015,7) have been examined

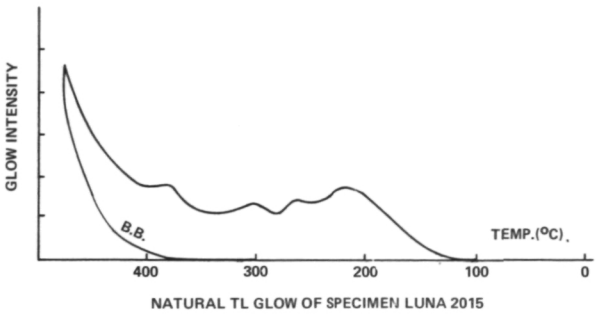

Figure 6.—*Natural TL glow of Luna 2015 specimen.*

for natural and induced thermoluminescence. The Luna 2015 specimen (yellowish gray in color) was collected at a depth of about 27 cm below ground-level and its natural thermoluminescence (fig. 6) was well preserved by the shielding of the top soil which attenuated the diurnal heat wave on the surface of the Moon.

The thermoluminescence induced in the L2015 sample has a glow spectrum similar to that of the Apollo samples studied. Its response to beta particles ($\sim$ 0.5 Ci, Sr-90) is linear up to about 1.2 megarads, where saturation begins. The response to gamma radiation ($\sim$ 200 Ci, Co-60) is similar to that induced by beta particles. The natural sample was exposed to five different gamma-ray doses ranging from 410 to 4500 kilorads by positioning aliquots at various distances from the γ source; the induced glows were measured for temperature regions of 0°–280° C, 280°–360° C, and 360°–480° C together with the total area. The 360°–480°C glow was used to estimate the effective storage temperature on the Moon, which was found to be 282 K at 27-cm depth. With the use of this result, the effective thermal wavelength for the depth concerned (27 cm) is estimated to be approximately 230 cm, about nine times the value previously assumed (refs. 8 and 23) for the surface samples.

The trapping parameter, energy depth, E, was determined by use of the initial rise technique; and approximate values for the corresponding frequency factor, S, were calculated (table 9). The high value for the frequency factor of the 150° C peak implies that this component is highly unstable at room temperature. The result is consistent with the finding of a fast decay component of all Apollo specimens.

Luna 1627 (darkish in color) showed very little preserved natural thermoluminescence; no glow was observed in the 0° C to 480° C region. The response to beta particles (0.5 Ci, Sr-90) of this specimen is about seven times smaller than that of Luna 2015. The emission spectrum of L1627 (fig. 7) also shows a number of different features compared with the other sample, implying that L1627 and L2015 have different compositions. The differences observed, together with the fact that very little thermoluminescence is exhibited by sample L1627, are consistent with the substantial quantities of glass and glassy material present. Similar results have been obtained for the well-known "orange soil"

Table 9.—*Thermoluminescence Trapping Parameters, Energy Depth, E, and Frequency Factor, S, for Various Peaks in the Natural Thermoluminescence Spectrum of L2015*

Peak Maximum (°C)	Energy Depth, E (ev)	Approximate Frequency Factor, S (sec^{-1})
90	0.91 ± 0.1	10^{12}
150	1.26 ± 0.1	4×10^{15}
210	1.16 ± 0.1	3×10^{11}
305	1.03 ± 0.1	10^{8}
370	1.17 ± 0.1	2×10^{8}

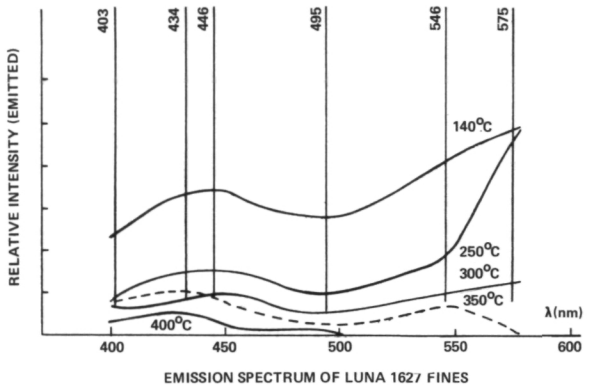

Figure 7.—*Emission spectrum of Luna 1627 fines.*

from the Apollo 17 mission, which also has a high glass content.

OXYGEN ISOTOPE ABUNDANCES IN FINE-SIZE FRACTIONS

Using "fluorine stripping" experiments, American and French workers have found large enrichments in ^{18}O (and ^{30}Si) on the surfaces of grains in certain samples of lunar soil. However, for Apollo 17 (ref. 24), Luna 16 (ref. 25), and Apollo 15 (ref. 26) there is not a simple monotonic decrease in ^{18}O content with the fraction of oxygen extracted.

Because the technique of "fluorine stripping" must, to some extent, mask the relationship between the content of ^{18}O and grain size, we have measured the abundance of ^{18}O in the total oxygen extracted from fine-size fractions of Luna 16 and Luna 20 soil. Approximately 10 mg of the $< 48\mu m$ fraction from the separation scheme were sieved in carbon tetrachloride into fractions of three sizes: $> 40\ \mu m$, 25–40 μm, and $< 25\ \mu m$. Samples of fractions of these sizes, weighing between 0.5 mg and 2.0 mg, have been analyzed with conventional BrF_5 extraction techniques and a high-precision mass spectrometer (ref. 9). The results are given in table 10a and b in standard δ notation per mil relative to SMOW (defined from Caltech Rose Quartz at + 8.45‰).

The results in table 10a are considered to be analytically accurate to within ± 0.1 to 0.2‰, and results obtained for the NBS 28 Quartz Standard (ref. 27) during the course of this work are listed in table 10b. However, it should be noted that prior to analysis the samples had not been subject to special handling precautions (they were in contact with

Table 10a.—*$^{18}O/^{16}O$ Determinations: Luna 16 and Luna 20 Sieved Fractions*

Sample	$< 25\ \mu$	25–40 μ	40–48 μ	Size of Fraction
Luna 16	+7.05‰	+8.76‰	+5.45‰	$\delta\ ^{18}O$ relative to SMOW
Luna 20	+7.44‰	+5.34‰	+7.47‰	

Table 10b.—*$^{18}O/^{16}O$ Determinations: Standards*

Sample	$\delta\ ^{18}O$ (SMOW) (per mil)
NBS 28 Quartz Standard	9.98, 10.00, 9.87, 10.15, 10.21, 9.98, 9.93 Mean 10.02 ± 0.11 (1 σ std. dev.)

the laboratory atmosphere, etc.) and Taylor and Epstein (ref. 28) have also suggested that polythene contamination may have affected their analysis of one aliquot of Luna 20 soil.

Epstein and Taylor (ref. 29) suggested that the observed surface enrichments are due to preferential loss of ^{28}Si and ^{16}O during fractional volatilization (or grain of ^{30}Si and ^{18}O during fractional condensation) resulting from bombardment of the lunar surface by meteorites and/or nuclear particles. Values for $\delta\ ^{18}O$ between about + 5.3‰ and + 6.3‰ can be regarded as normal for bulk samples of lunar soil. The results presented in table 10a show that grain sizes other than the finest are also enriched in ^{18}O. Such variations in ^{18}O enrichment with grain size are readily understood if the soil at each locality is a mixture of young and mature grains. Mature grains (showing ^{18}O enrichment) in particular grain size fractions may be acquired from impact events at differing distances from the sample localities.

CHARGED PARTICLE TRACKS

Charged particle track analysis has been carried out to study the exposure and mechanical histories of a brown glass speck (~ 0.5 mm across) from the Luna 16 soil (L1627,3,1C).

Because of the roughness of the surface, no craters or features attributable to compositional differences could be recognized from a preliminary examination of the grain. However, the optical microscope showed a high density of bubbles (~ 10^5 bubbles/ cm^2) distributed throughout the body of the speck. A more thorough examination of the bubble distribution showed a maximum density in the center of the body and a minimum near the surfaces. Thus, the gas bubbles were probably migrating outward at the time of solidification of the glass.

Annealing experiments were carried out on a part of the speck in order (a) to study the annealing characteristics of the latent damage tracks, and (b) if possible, to utilize the results from (a) to separate the genuine track density from the background pits. The sample was annealed for 10-minute periods at various temperatures from 200° C to 700° C and then etched in 4.8 percent solution of HF for 5 seconds at 21 ± 0.5° C, prior to track density measurement by scanning electron microscope (SEM). It was found that (a) almost all the genuine tracks were annealed out at ~ 550° C, (above this temperature highly stable pits due to background were left (ref. 30)) and (b) the genuine track density to background pit ratio was 14.

Experiments were also carried out to study the track registration and development properties of the glass, and it was found that the track registration properties of the glass

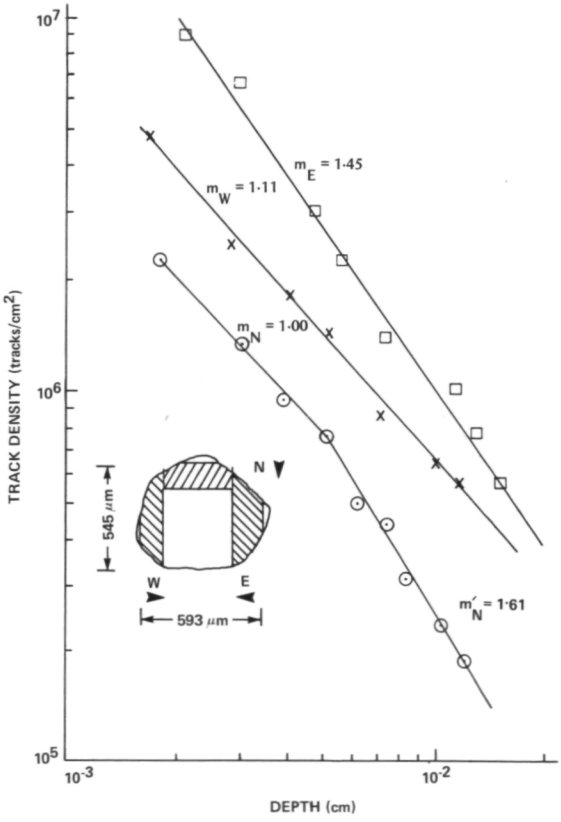

Figure 8.—*Variation of track density (tracks/cm²) with depth on three different faces (E, W, N, as shown in the inset) of a brown glass speck from Luna 16 sample, 1627,3,1C. The tracks were produced mainly by solar flares.*

were very similar to tektite and obsidian glasses (ref. 31).

The major portion of the glass speck was mounted in resin on a quartz backing and then polished and etched as previously described. The tracks were observed and counted by using the SEM. The track densities were determined at various depths; the whole process was repeated on three different faces of the glass (fig. 8). The results (fig. 8) show that all three faces examined have track density gradients, and a relation of the type $\rho_D = \rho_0 D^{-m}$ seems to exist (where ρ_0 and ρ_D are the track densities on the surface and at depth "D," respectively, and "m" is the coefficient showing the nature of the charged particle spectrum). The value of the coefficient "m" is modified by various factors such as the presence or absence of some soil layer on the grain observed, its burial depth, and the extent of erosion due to charged particle and micrometeoritic bombardments. Faces "E" and "W" yield values for coefficient "m" of 1.45 and 1.11, respectively, while there are two "m" values (1.00 and 1.61) for the face "N." This shows that faces "E" and "W" had simple burial histories, while the burial history of face "N" is somewhat complicated. Thus, the above results suggest that the glass speck remained for most of its life on or near to the lunar surface and that it had at least three orientations. In general, the Luna 16 site seems to be highly irradiated and well churned.

CARBON CHEMISTRY

Dissolution of fractions in DCl (38 percent in D_2O) has been used to measure the trapped CH_4 and the hydrolysable carbon (as indicated by the evolution of CD_4) presents. In general, the results obtained from Luna 16 and 20 (tables 11 and 12) are comparable with those from similar fractions of Apollo 11 and 16, respectively (ref. 11).

Table 11.—*CD_4 and CH_4 Released by DCl Dissolution of Selected Fractions of Luna 16 and 20 Fines* [1]

Sample Description	Sample Daughter Number	Luna 16			Luna 20		
		CD_4 (μg/g as C)	CH_4 (μg/g as C)	CD_4/CH_4	CD_4 (μg/g as C)	CH_4 (μg/g as C)	CD_4/CH_4
Bulk Sample	1	19.3	3.0	6.4	10.9	4.8	2.3
>250 μm (handpicked agglutinates)	3	12.1	0.86	14.1	n.m.[2]	n.m.	n.m.
48–250 μm (washed)	8	19.3	2.7	7.1	4.4	1.7	2.6
<48 μm	7	18.8	5.7	3.3	8.0	5.3	1.5
Finest Fines (<10 μm)	9	19.2	6.2	3.1	15.9	8.9	1.8

NOTES: (1) Notation on errors—absolute amounts of CD_4 and CH_4 are measured to $\pm$ 10 percent; CD_4/CH_4 ratio $\pm$ 2 percent, based on peak height.
(2) In each use, n.m. indicates equivalent fraction from L20 not available in quantities sufficient for analysis.

Table 12.—*CD_4 and CH_4 Released by DCl Dissolution of Density and Magnetically Separated Fractions (48–250μm) of Luna 16 and 20 Fines* [1]

Sample Parent Number	Sample Daughter Number	Density (g/cm³)	d (cm) [2]	CD_4 (μg/g as C)	CH_4 (μg/g as C)	CD_4/CH_4 [3]
L1627,10,2	1	< 2.96	0.25–0.35	n.c. [4]	n.c.	11.9
L1627,10,2	2	< 2.96	0.05–0.25	n.c.	n.c.	9.5
L1627,10,2	3	< 2.96	0.0 –0.05	n.c.	n.c.	10.5
L1627,11,2	1	> 2.96	0.2 –0.25	n.c.	n.c.	5.2
L2015,10,2	1	< 2.78	n.s. [5]	7.2	1.6	4.5
L2015,11,2	1	> 2.78	n.s.	1.5	0.85	1.8

NOTES: (1) Concentration of CD_4 and CH_4 in unseparated washed fines (48–250μm) L1627,10 are 19.3 and 2.7 μg/g, respectively, with $CD_4/CH_4 = 7.1$. Concentration of CD_4 and CH_4 in unseparated washed fines (48–250μm) L2015,10 are 4.4 and 1.7 μg/g, respectively, with $CD_4/CH_4 = 2.6$.
(2) Vertical distance between sample and tip of magnetized soft iron rod, d = 0 means sample touching soft iron.
(3) Errors for CD_4/CH_4 ratio measurement ± 2%.
(4) In each use, n.c. indicates not calculated, sample size analyzed insufficiently to allow estimation of absolute amounts of CD_4 and CH_4 to greater accuracy than ± 50%.
(5) In each use, n.s. indicates not separated.

The formation of the hydrolysable carbon giving rise to CD_4 in lunar fines is dependent on both surface exposure and the availability of Fe^{II} in the soil (for reduction to free Fe^0 in particle surfaces and agglutinates (refs. 32 and 33).

Magnetic susceptibility, X_i, is a measure of free Fe^0. The direct relationship between Fe^0 and the degree of exposure and Fe^{II} content established for lunar soils is also apparent from the data for X_i and CD_4 for various fractions (> 10μm) of Luna 16 and 20 soils (tables 7, 11, and 12). Thus, taking into consideration the lower total Fe^{II} content of Luna 20 (the total iron contents of Luna 16 and 20 are 16.3 percent and 7.0 percent (as FeO), respectively (refs. 1 and 2)) the amounts of CD_4 released from bulk materials (as shown in table 11) indicate that both soils are very mature and have experienced a similar degree of exposure on the lunar surface.

The ratio (CD_4/CH_4) of involatile carbon (hydrolysable carbon) to volatile carbon (CH_4) reflects both the Fe^{II} content and the degree of recycling of grains into complex particles. Thus, high CD_4/CH_4 ratios (tables 11 and 12) are observed for agglutinate-rich fractions (handpicked fraction of Luna 16 agglutinates, the low-density/highly magnetic fractions of Luna 16, and low-density fraction of Luna 20). The CD_4/CH_4 ratio of 6.4 measured for the bulk Luna 16 fines is consistent with the higher proportion of glasses and agglutinates present in this soil as compared with Luna 20 ($CD_4/CH_4 = 2.3$).

The analysis of size-separated fractions (table 11) shows that for both Luna soils, the CH_4 concentration increases as particle size decreases, as previously observed for the Apollo 11 fines (ref. 10) and the Apollo 14 soils (ref. 34). Also, for Luna 20, hydrolysable carbon is present in the largest quantities in fine-grained fractions. In contrast, for Luna 16 sieved fractions the carbide con-

centration is virtually independent of grain size, suggesting a considerable volume-related hydrolysable carbon component, again in accord with the much greater abundance of complex particles aggregated from fine, exposed grains (ref. 10). One explanation may be that the rate of particle aggregation at the Luna 16 site was rapid relative to the rate of hydrolysable carbon synthesis in fine grains, as has been suggested in reference 35 for total carbon accumulation in mature samples.

For both Luna 16 and Luna 20, the finer fractions ($< 48\mu$m) have lower CD_4/CH_4 ratios and higher absolute amounts of CH_4 relative to the fractions which contain larger grains (bulk samples $> 250\mu$m, 48–250μm, table 11). These low ratios could suggest that the fine fractions contain few "complex particles," i.e., those which have undergone fractionation of the carbonaceous species during formation.

It has previously been suggested that ultrafine grains are the primary site for CH_4 and hydrolysable carbon synthesis (refs. 11 and 12). If these particles are relatively simple, then the CD_4/CH_4 ratios must reflect the relative rates of formation of hydrolysable carbon and CH_4 within the constituent silicate matrix and should be low. Hence, the high CH_4 concentrations in low Fe^{II} soil (Luna 20) suggest that the synthesis of the hydrocarbon in fine grains, unlike carbide, does not involve the availability of Fe^{II} within the sample (ref. 36).

Alternatively, if complex particles are present in fractions $< 48\mu$m, from aggregation of smaller particles or disaggregation of larger complex particles, other interpretations have to be considered. *Either* (a) small complex particles have not suffered the changes in carbon chemistry observed in large complex particles (glassy agglutinates), *or* (b) whatever the nature of the particle, provided it is very small, solar wind exposure effects (formation of CH_4, etc.) are dominant and generally obliterate the previous history. The last proposition is most appropriate for the ultrafine grains being the primary site for CH_4 and hydrolysable carbon synthesis.

Conclusions

A concerted analysis of Luna 16 and Luna 20 soils has been carried out. In order to obtain the maximum information from the small samples available, only fractions appropriate to a particular technique have been analyzed by that technique. Some fractions have been subdivided into aliquots and thus data obtained may be considered completely interrelatable.

The conclusions are as follows:

1. Luna 16 is typical of mare material, wheras Luna 20 is typically highland in origin; little or no highland-type glass occurs in Luna 16 and only very rare fragments of mare composition material are present in Luna 20. Both soils are similar to their appropriate Apollo counterparts, Apollo 11 and 16, respectively.
2. Exposure measurements (carbon chemistry and $^{38}Ar/^{37}Ar$ measurements) and petrology confirm that both soils are highly mature and well gardened. The higher quantities of free iron (magnetic and Mössbauer measurements) and hydrolysable carbon (carbon chemistry) observed within the mare soil are in agreement with the postulated origin of these species by exposure-induced reduction of indigenous Fe^{II} in lunar silicates rather than from an input of meteorite debris.
3. Petrology, Mössbauer spectroscopy, thermoluminescence studies, and carbon chemistry data all suggest that a greater proportion of glass and glassy materials (such as agglutinates) is present in Luna 16 samples compared with Luna 20, presumably because of the lower temperature required to melt rocks and minerals of mare origin. The relatively higher proportions of CH_4 in fractions of highland material (Luna 20) which contains the least numbers of complex or recycled grains suggest that CH_4, unlike hydrolysable carbon, is independent of the Fe^{II} content of the silicate.

4. A very high gas retention age (4.3–4.4 Gy) has been recorded for a sample of Luna 20 soil consisting of several handpicked fragments of cataclastic anorthosites, and has identified early crustal material which existed prior to the Imbrium event. A number of ages in the range of 4.0 to 4.3 Gy have been reported for A16 and A17 samples (refs. 37, 38, and 39). This is the only pre-Imbrium sample detected at the Luna 20 site so far. Clearly, more favorable samples should be selected from the bulk of the Luna 20 material, and further studies performed.

Acknowledgment

The authors wish to thank the Soviet Academy of Sciences for providing the samples of Luna 16 and 20 material for study. Appreciation also is expressed to the Royal Society for sponsorship and a grant to enable sample processing to be carried out. The sample analyses were made possible by grants from the Science Research Council and the Natural Environment Research Council. Further acknowledgments with thanks are given to the British Steel Corporation for providing a Fellowship to C.T. Pillinger; and to Mr. B. Scarlett of the University of Technology, Loughborough, for supplying the sieved fractions for oxygen isotope measurements.

References

1. VINOGRADOV, A. P., Preliminary Data on Lunar Ground Brought to Earth by Automatic Probe "Luna-16." *Proc. Second Lunar Science Conference, Geochimica et Cosmochimica Acta,* Supplement 2, Vol. 1, 1971, pp. 1–16.
2. VINOGRADOV, A. P., Preliminary Data on Lunar Soil Collected by the Luna 20 Unmanned Spacecraft. *Geochimica et Cosmochimica Acta,* Vol. 37, 1973, pp. 721–729.
3. ABELL, P. I., G. H. DRAFFAN, G. EGLINTON, J. M. HAYES, J. R. MAXWELL, AND C. T. PILLINGER, Organic Analysis of the Returned Lunar Sample. *Proc. Apollo 11 Lunar Science Conference, Geochimica et Cosmochimica Acta,* Supplement 1, Vol. 2, 1970, pp. 1757–1773.
4. TURNER, G., P. H. CADOGAN, AND C. J. YONGE, Argon Selenochronology. *Proc. Fourth Lunar Science Conference, Geochimica et Cosmochimica Acta,* Supplement 4, Vol. 2, 1973, pp. 1889–1914.
5. COLLINSON, D. W., AND A. DE SA, A New Magnetometer for Small Scale Magnetic Studies. *J. Phys. E.,* Vol. 4, 1971, pp. 337–341.
6. GIBB, T. C., R. GREATREX, N. N. GREENWOOD, AND M. H. BATTEY, Mössbauer Studies of Apollo 14 Lunar Samples. *Proc. Third Lunar Science Conference, Geochimica et Cosmochimica Acta,* Supplement 3, Vol. 3, 1972, pp. 2479–2493.
7. GIBB, T. C., R. GREATREX, AND N. N. GREENWOOD, Mössbauer Studies of Apollo 14 and Apollo 15 Lunar Soils. *J. C. S. Dalton,* in press, 1974.
8. DURRANI, S. A., W. PRACHYABRUED, C. CHRISTODOULIDES, J. H. FREMLIN, J. A. EDGINGTON, R. CHEN, AND I. M. BLAIR, Thermoluminescence of Apollo 12 Samples: Implications for Lunar Temperature and Radiation Histories. *Proc. Third Lunar Science Conference, Geochimica et Cosmochimica Acta,* Supplement 3, Vol. 3, 1972, pp. 2955–2970.
9. BECKINSALE, R. D., N. J. FREEMAN, M. C. JACKSON, R. E. POWELL, AND W. A. P. YOUNG, A 30 cm radius 90° Sector Doubled Collecting Mass Spectrometer With a Capacitor Integrating Detector for High Precision Isotopic Analysis of Carbon Dioxide. *Int. J. Mass Spectrom. and Ion Phys.,* Vol. 12, 1973, pp. 299–308.
10. CADOGAN, P. H., G. EGLINTON, J. N. M. FIRTH, J. R. MAXWELL, B. J. MAYS, AND C. T. PILLINGER, Survey of Lunar Carbon Compounds: II. The Carbon Chemistry of Apollo 11, 12, 14 and 15 Samples. *Proc. Third Lunar Science Conference, Geochimica et Cosmochimica Acta,* Supplement 3, Vol. 2, 1972, pp. 2069–2090.
11. CADOGAN, P. H., G. EGLINTON, J. R. MAXWELL, AND C. T. PILLINGER, Distribution of Methane and Carbide in Apollo 11 Fines. *Nature Phys. Sci.,* Vol. 241, 1973, pp. 81–82.
12. CADOGAN, P. H., G. EGLINTON, A. P. GOWAR, A. J. T. JULL, J. R. MAXWELL, AND C. T. PILLINGER, Location of Methane and Carbide in Apollo 11 and 16 Lunar Fines. *Proc. Fourth Lunar Science Conference, Geochimica et Cosmochimica Acta,* Supplement 4, Vol. 2, 1973, pp. 1493–1508.
13. WARNER, J., A. M. REID, W. I. RIDLEY, AND R. W. BROWN, Major Element Composition of Luna 20 Glass. *Earth Planet. Sci. Letters,* Vol. 17, 1972, pp. 6–12.
14. EL GORESY, A., L. A. TAYLOR, AND P. RAMDOHR, Fra Mauro Crystalline Rocks: Mineralogy, Geochemistry and Subsolidus Reduction of Opaque Minerals. *Proc. Third Lunar Science Conference, Geochimica et Cosmochimica Acta,* Supplement 3, Vol. 1, 1972, pp. 333–349.

15. PODOSEK, F. A., J. C. HUNEKE, A. J. GARCARZ, AND G. J. WASSERBURG, The Age and Petrography of Two Luna 20 Fragments and Inferences for Widespread Lunar Metamorphism. *Geochimica et Cosmochimica Acta*, Vol. 37, 1973, pp. 887–904.
16. STEPHENSON, A., Single Domain Grain Distributions: I. A Method for the Determination of Single Grain Distributions. II. The Distribution of Single Domain Iron Grains in Apollo 11 Lunar Dust. *Phys. Earth Planet. Interiors*, Vol. 4, 1971, pp. 353–369.
17. RUNCORN, S. K., D. W. COLLINSON, W. O'REILLY, M. H. BATTEY, A. STEPHENSON, J. M. JONES, A. J. MANSON, AND P. W. READMAN, Magnetic Properties of Apollo 11 Lunar Samples. *Proc. Apollo 11 Lunar Science Conference, Geochimica et Cosmochimica Acta*, Supplement 1, Vol. 3, 1970, pp. 2369–2387.
18. MALYSHEVA, T. V., Mössbauer Spectroscopy of Lunar Regolith Returned by the Automatic Station Luna 16. *Proc. Third Lunar Science Conference, Geochimica et Cosmochimica Acta*, Supplement 3, Vol. 1, 1972, pp. 105–114.
19. MALYSHEVA, T. V., AND V. V. KURASH, Mössbauer Spectroscopy of Lunar Samples. *Geochem. Internat.*, Vol. 87, 1973.
20. VINOGRADOV, A. P., Preliminary Data on Lunar Regolith Returned by Automatic Probe "Luna-20." *Geochem. Internat.*, 1972, p. 507.
21. MALYSHEVA, T. V., Mössbauer Spectroscopy of a Lunar Regolith Supplied by the Luna 20 Automatic Space Station. *Geokhimiya*, 1973, p. 1079.
22. BANNERJEE, S. K., W. O'REILLY, T. C. GIBB, AND N. N. GREENWOOD, The Behaviour of Ferrous Ions in Iron-Titanium Spinels. *J. Phys. and Chem. Solids*, Vol. 28, 1967, p. 1323.
23. DURRANI, S. A., W. PRACHYABRUED, F. S. W. HWANG, J. A. EDGINGTON, AND I. M. BLAIR, Thermoluminescence of Some Apollo 14 and 16 Fines and Rock Samples. *Proc. Fourth Lunar Science Conference, Geochimica et Cosmochimica Acta*, Supplement 4, Vol. 3, 1973, pp. 2465–2479.
24. EPSTEIN, S., AND H. P. TAYLOR, O^{18}/O^{16}, Si^{30}/Si^{28}, C^{13}/C^{12}, D/H and Hydrogen and Carbon Concentration Data on Apollo 17 Soils. *Eos*, 1973, pp. 585–586.
25. JAVOY, M., J. MARETTE, AND F. PINEAU, $^{18}O/^{16}O$ Ratios in Luna 16 Fines. *Geochimica et Cosmochimica Acta*, Vol. 37, 1973, pp. 2017–2019.
26. JAVOY, M. AND S. FOURCADE, $^{18}O/^{16}O$ Ratios in Lunar Fines and Rocks. *Earth Planet. Sci. Letters*, Vol. 21, 1974, pp. 377–382.
27. FRIEDMAN, I. AND J. D. GLEASON, A New Silicate Intercomparison Standard for ^{18}O Analysis. *Earth Planet. Sci. Letters*, Vol. 18, 1973, p. 124.
28. TAYLOR, H. P., AND S. EPSTEIN, Oxygen and Silicon Isotope Ratios of the Luna 20 Soil. *Geochimica et Cosmochimica Acta*, Vol. 37, 1973, pp. 1107–1109.
29. EPSTEIN, S. AND H. P. TAYLOR, O^{18}/O^{16}, Si^{30}/Si^{28}, C^{13}/C^{12} and D/H Studies of Apollo 14 and 15 Samples. *Proc. Third Lunar Science Conference, Geochimica et Cosmochimica Acta*, Supplement 3, 1972, pp. 1429–1454.
30. KHAN, H. A., On Thermal Annealing of Latent Damaged Trails. *Radiation Effects*, Vol. 18, 1973, pp. 51–54.
31. KHAN, H. A., AND S. A. DURRANI, Efficiency Calibration of Solid State Nuclear Track Detectors. *Nuclear Instruments and Methods*, Vol. 98, 1972, pp. 229–236.
32. PILLINGER, C. T., B. D. BATTS, G. EGLINTON, A. P. GOWAR, A. J. T. JULL, AND J. R. MAXWELL, Formation of Lunar Carbide From Lunar Iron Silicate. *Nature Phys. Sci.*, Vol. 245, 1973, pp. 3–5.
33. PILLINGER, C. T., P. R. DAVIS, G. EGLINTON, A. P. GOWAR, A. J. T. JULL, J. R. MAXWELL, R. HOUSLEY, AND E. H. CIRLIN, The Association Between Carbide and Finely Divided Metallic Iron in Lunar Fines. *Proc. Fifth Lunar Science Conference, Geochimica et Cosmochimica Acta*, Supplement 5, in press, 1974.
34. HOLLAND, P. T., B. R. SIMONEIT, P. C. WSZOLEK, AND A. L. BURLINGAME, Compounds of Carbon and Other Volatile Elements in Apollo 14 and 15 Samples. *Proc. Third Lunar Science Conference, Geochimica et Cosmochimica Acta*, Supplement 3, Vol. 2, 1972, pp. 2131–2148.
35. DESMARAIS, D. J., J. M. HAYES, AND W. G. MEINSCHEIN, Accumulation of Carbon in Lunar Soils. *Nature Phys. Sci.*, Vol. 246, 1973, pp. 65–68.
36. PILLINGER, C. T., P. R. DAVIS, G. EGLINTON, A. P. GOWAR, A. J. T. JULL, AND J. R. MAXWELL, Unpublished results, 1974.
37. SCHAEFFER, O. A., AND L. HUSAIN, Early Lunar History: Ages of 2–4 mm Soil Fragments From the Lunar Highlands. *Proc. Fourth Lunar Science Conference, Geochimica et Cosmochimica Acta*, Supplement 4, Vol. 2, 1973, pp. 1847–1863.
38. KIRSTEN, T., AND P. HORN, ^{39}Ar-^{40}Ar Chronology of the Taurus-Littrow Region II: A 4.28 b.y. Old Troctolite and Ages of Basalts and Highland Breccias. *Lunar Science*, Vol. V, 1974, pp. 419–421.
39. STETTLER, A., P. EBERHARDT, J. GEISS, GRÖGLER, AND P. MAURER, Sequence of Terra Rock Formation and Basaltic Lava Flows on the Moon. *Lunar Science*, Vol. V, 1974, pp. 738–740.